ARID ZONE JOURNAL OF ENGINEERING, TECHNOLOGY & ENVIRONMENT
AZOJETE June 2025. Vol.21(2):646-655
Published by the Faculty of Engineering, University of Maiduguri, Maiduguri, Nigeria.
Print ISSN: 1596-2490, Electronic ISSN: 2545-5818
https://doi.org/10.63958/AZOJETE/2025/21/02/029
www.azojete.com.ng

ORIGINAL RESEARCH ARTICLE

EFFECT OF OIL PALM BIOMASS CELLULOSIC CONTENT ON MOLECULAR STRUCTURE OF BIOCHAR

A. A. Lawal [1*], M. A. Hassan [2,3], B. Mohammed [1], and Y. Shirai [4]

[1]*Department of Agricultural and Environmental Resources Engineering, Faculty of Engineering, University of Maiduguri, Maiduguri, Borno State, Nigeria*
[2]*Department of Process and Food Engineering, Faculty of Engineering, Universiti Putra Malaysia, 43400 UPM Serdang, Selangor, Malaysia*
[3]*Department of Bioprocess Technology, Faculty of Biotechnology and Biomolecular Sciences, Universiti Putra Malaysia, 43400 UPM Serdang, Selangor, Malaysia*
[4]*Department of Biological Functions and Engineering, Graduate School of Life Science and Systems Engineering, Kyushu Institute of Technology, 2-4 Hibikino, Wakamatsu-ku, Kitakyushu, Fukuoka 808-0196, Japan*
* *Corresponding author's email: abubakar.lawal@unimaid.edu.ng*

ARTICLE INFORMATION

Received: 19th February 2025
Revised: 11th April 2025
Accepted: 12th April 2025

Keywords:
Cellulosic content
Biochar
Surface functionality
Thermal stability

ABSTRACT

Biochar is attractive mainly due to its diverse surface functionality bringing the possibility of multipurpose utilization. The purpose of this study was to evaluate the effect of biomass cellulosic content on evolution of molecular structures of biochar. Commercial cellulose, oil palm front, and palm kernel shell were pyrolyzed at 630 °C, and their biochar structures were analyzed using ultimate and proximate compositions, pH point of zero charge, FTIR and XRD. Evaluation of biochar nanotexture based on cellulosic content (100% for commercial cellulose, 39.5% for oil palm front and 20.5% for palm kernel shell) revealed that commercial cellulose decomposed rapidly into non-graphitizing large size crystallites (65 nm) with substantial defects within their graphene sheets. The thermal decomposition mechanism for cellulose and lignin differs: cellulose decomposed rapidly to form O heterocyclic rings before final phase transition to graphene sheets at a much lower temperature, whereas lignin decomposed slowly and begins forming graphene sheets after series of condensation reactions at higher temperatures. Amorphous chars derived from lignin were thermally stable, slowing down the rapid formation of crystallites in biochar from palm kernel shell. Conclusively, highly cellulosic biomass is highly thermally unstable and tends to decomposed into biochar with lower surface functionality compared to biochar derived from highly lignified biomass.

1.0 Introduction

Recently, the global oil palm industry has growing interest on converting the huge amounts of oil palm biomass residues it generated into value-added products aiming at achieving zero-waste emission in the mills, and a more sustainable and profitable palm oil industry (Ali *et al*., 2015). Accordingly, there is increasing interest and attention on producing biochar from the residues for a number of applications. A variety of oil palm biomass residues have been considered for biochar production: palm kernel shell, mesocarp fibre, empty fruit bunch, palm kernel cake, palm oil mill sludge, frond and trunk (Kong *et al*., 2014). However, despite the abundance of the residues, selecting biomass precursor capable of producing a biochar with specific functionality using simple environmentally friendly production method such as pyrolysis has always been challenging.

The nature of feedstock used for producing biochar is an influential factor that contributes to nature of char formed during pyrolysis. In order words, the proportion of feedstock components (i.e., biopolymers) and their conformation could have a considerable effect on the extent of the evolved biochar structure and functionality. During thermal decomposition of biomass, it is expected that restructuring and re-organization processes of the decomposing biopolymers would lead to the evolution of carbon rich materials, identified as pyrogenic

chars known as the biochar nanotexture. Keiluweit *et al.* (2010) conducted a molecular-level assessment study of the physical organization of biomass-derived biochar and observed a transition of the biomass, as it thermally decomposed, from transition chars to turbostratic char and also noticed a gradual increase in surface area with increasing proportions of turbostratic crystallites embedded in amorphous char. Consequently, knowledge of the proportion of feedstock components and their conformation, along with their thermal decomposition behaviour, will assist in the selection of feedstock that can produce high porosity and unique functionality. Although a lot of research have been conducted on converting oil palm biomass into biochar (Abd Waft *et al.*, 2017; Jia and Lua, 2008; Zainal *et al.*, 2018, Amosa *et al.*, 2014; Parthasarathy *et al.*, 2016; Rugayah *et al.*, 2014), little is known about the contribution of lignocellulosic components on the functionality of biochar. Correlation between the components of feedstock and biochar functionality will guide in the production of engineered biochar suitable for specific applications. Therefore, the objective of this study was to assess the effect of cellulosic content on the evolution of pyrogenic molecular structure of oil palm biomass derived-biochar.

2. Materials and Method

2.1 Pretreatment of Feedstocks

The oil palm frond, palm kernel shell, and commercial cellulose used in this study were collected from different sources. About 1 kg of fresh oil palm fronds were collected from Universiti Putra Malaysia oil palm plantation and transported to the Biomass and Biorefinery Center of the university. The fresh fronds were sliced into rectangular pieces approximately 5 cm long, 3 cm width, and 2 cm thick and dried in an electric drying oven (Mmmert, Germany) at 105 °C for 72 h to remove moisture and avoid the decay of the fresh fibre. Approximately 500 g of dried palm kernel shell was collected from FELDA Palm Oil Mill, Pasoh, Negeri Sembilan, and transported to the Biomass and Biorefinery Center. The shells collected were soaked in distilled water for 10 h before squeezing and washing with distilled water to remove impurities. The clean shells were dried in an electric drying oven (Memmert, Germany) at 105 °C for 72 h. About 500 g of commercial cellulose was purchased from R&M chemicals. The dried samples were stored in designated airtight plastic bags (Figure 1). Powdery samples used for feedstock characterization were prepared by chopping about 50 g into pieces and ground in a wood grinder to pass through a 425 µm sieve (40 US mesh screen). The following chemicals purchased from Merck were used to determine cellulose, hemicellulose and lignin, and pH_{PZC} of the biomass materials: $NaClO_2$, H_2SO_4, $NaNO_3$, HNO_3 and NaOH.

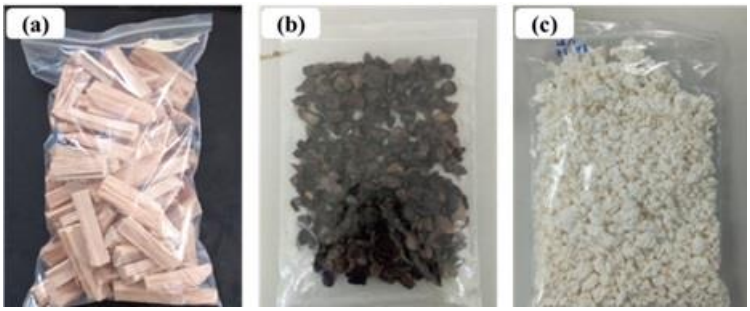

Figure 1: Feedstocks: (a) oil palm frond, (b) oil palm kernel shell, (c) commercial cellulose

2.2 Biochar Production

Nitrogen pyrolysis was conducted to produce biochar from oil palm frond, palm kernel shell, and commercial cellulose. The nitrogen pyrolysis test is frequently used as a means for studying the structure of biochar formed during carbonization. The basic principle of the test is to heat biomass at a high temperature in the presence of flowing nitrogen and measure the relevant physicochemical properties of the biochar produced. Therefore, the nitrogen pyrolysis test used in this research followed the procedure reported by Keiluweit *et al.* (2010) and Cao *et al.* (2012). In this study, about 30 g each of the oil palm frond, oil palm kernel shell, and commercial cellulose were carbonized separately using the dual-mode pyrolysis system. In a nitrogen gas flow rate of 100 cm^3/min, the feedstocks were heat-treated at a heating rate of 40 °C/min to 630 °C for an hour before cooling down to room temperature. The biochars produced were gently pulverized using pestle and mortar made from stainless steel to pass through a 250 µm sieve (60 US mesh screen). The powdered biochars produced from commercial cellulose, oil palm frond, and palm kernel shell were placed and sealed in designated vessels CC-BC, OPF-BC, and PKS-BC, respectively.

Corresponding author's email address: abubakar.lawal@unimaid.edu.ng

2.3 Biopolymer, Proximate, and Ultimate Compositions

The fraction of the biopolymers in each fibre was determined based on the method developed by Norrrahim *et al.* (2018). Lignin was first removed by soaking a fibre in 5 wt. % $NaClO_2$ solution adjusted with H_2SO_4 to a pH between 4 and 5. After an hour of soaking at 70 °C, the fibre was washed with deionized water until neutral pH. Hemicellulose was removed from the by soaking the lignin-free fibre in 6 wt. % KOH solution at 25 °C for 24 h. The fractions (dry basis) of cellulose, hemicellulose, and lignin in the fibre were calculated from their respective weights. The weight-loss behaviour was analyzed in a TGA-4000 thermogravimetric analyzer (PerkinElmer Instruments, USA). In each test, 15 mg of a sample was heated at 10 °C/min to 950 °C. Both the weight-loss curve and the derivative thermogravimetric curve were analyzed for the thermal characteristics of the feedstocks.

The proximate analysis was performed following the modified standard method for proximate analysis D3175-07 and D3174-04 (Cantrell *et al.*, 2010). The test was carried out in a TGA-4000 thermogravimetric analyzer (PerkinElmer Instruments, USA). Dry samples with particle size < 0.425 mm were used for the analysis. The sequential determination of moisture and volatile matter involved loading about 15 to 20 mg of sample into a ceramic crucible and heating to110 °C for 15 min in the presence of nitrogen gas flowing at 80 mL/min to liberate moisture. Removal of the volatile matter was carried out in an inert environment, and it involved heating the dry sample from 110 °C to 950 °C and isothermal hold for 7 min before rapid cool down to 110 °C. The heat treatment for ash content analysis was performed in the presence of zero-grade air flowing at 80 mL/min. The heat treatment involved heating the moisture free sample (15 to 20 mg) from 110 °C to 950 °C at 11 °C/min, followed by an isothermal hold for 10 min and rapid cooling to 110 °C. The percentage of moisture, volatile matter, and ash were calculated based on Equation 1, 2, and 3, respectively, while the percentage fixed carbon was calculated by difference using equation 4:

$$MC\ \% = (\text{mass loss at } 110\ ^\circ C/\text{mass of sample}) \times 100 \quad (1)$$

$$VM\ \% = (\text{mass loss at } 950\ ^\circ C/\text{mass of dry sample}) \times 100 \quad (2)$$

$$A\ \% = (\text{mass loss during air combustion/mass of dry sample}) \times 100 \quad (3)$$

$$FC\ \% = 100 - (MC\ \% + VM\ \% + A\ \%) \quad (4)$$

where MC % is percentage moisture, VM % percentage volatile, and A % percentage ash. The percentage composition of carbon, hydrogen, and nitrogen in biomass feedstocks and biochars was obtained from CHN analysis in the CHN628 analyzer (LECO, UK). The percentage composition of oxygen was calculated by difference.

2.4 Surface Functionality

Fourier-Transformed Infrared (FTIR) spectroscopy was performed in a Perkin-Elmer Spectrum GX FT-IR System instrument (Perkin-Elmer) to identify surface functional groups qualitatively. The principle of measurement involved mixing and pressing dry sample with potassium bromide at 1:100 to form a transparent compact disc and exposing it to infrared radiation within the wavelength range between 4000 to 400 cm^{-1} with each sample scanned 16 times. To understand the molecular structure of a biochar, the FTIR spectrum was analyzed at regions corresponding to OH, CH, C=C, and C=O groups and the fingerprint.

The procedure for determining the surface pH of the biochars produced in this study involved mixing 0.2 g of dry biochar with 10 mL of distilled water followed by agitation for 24 h to reach equilibrium before measuring the pH of the suspension using pH meter LAQUAtwin S010 (HORIBA, Japan) (Nowicki et al., 2015).

The pH point of zero charge (pH_{PZC}) was determined following the modified pH drift method by Mahmood *et al.* (2011). The pH_{PZC} determines the pH at which the surface of biochar is zero, where an increase in pH leads to a negatively charged surface. The pH drift method was carried out by mixing 0.1 g biochar with 20 mL of 0.1 M $NaNO_3$ solution in a vessel, and the pH of the suspensions was adjusted to 3, 4, 5, 6, 7, 8, 9, and 10 with either HNO_3 or NaOH. The pH of the suspension after 72 h of agitation was measured, and the difference between the final and initial pH (ΔpH) was plotted against the initial pH. The pH_{PZC} was determined to be the initial pH at which ΔpH was zero.

Corresponding author's email address: abubakar.lawal@unimaid.edu.ng

2.5 Morphology and Structure

Electron micrographs scanned at different magnifications were obtained using a scanning electron microscopy Hitachi S-3400 (Hitachi, Japan) for image analyses of particle sizes and surface morphology, respectively. Dry samples were coated with gold and scanned in the microscopy at 5 kV for image acquisition. The scanned images at low magnifications were subjected to qualitative particle size analysis, while the high magnification images were used for the analysis of surface morphology.

The crystalline structure of the biochars was analyzed using X-ray diffractometry. The powdered X-ray diffraction (XRD) method detects the presence of carbon crystallites in biochar microtexture based on their diffraction pattern in response to incident X-rays. XRD diffraction patterns for the biochars were recorded using a Shimadzu Diffractometer (XRD 6000, Japan) with a Cu Kα radiation at a wavelength, λ of 0.1541838 generated at 30 kV and 30 mA. The XRD diffraction was measured over the range 5° < 2 theta < 70° using the step-scanning method at 2 degrees/min step and sampling pitch of 0.02 degree. The 2 theta angle range was chosen to capture the reflection of the crystallographic basal plane (i.e., 002 indices) and the crystallographic reflection planes perpendicular to the basal planes (i.e., 10 indices).

The Origin 2018 Pro software was applied to the XRD patterns to extract constants relevant in calculating structural properties. The crystallites' structural parameters were calculated using known established expressions. The interlayer spacing between the graphene sheets, d_{002} and carbon crystallite thickness, L_c and diameter, L_a the average number of graphene sheets per carbon crystallites, n_s and the average number of carbon atoms per graphene sheet were calculate using Bragg's equation, Sherrer's emperical equations and Diamond's equation (Equations 5 to 9).

$$d_{002} = \frac{\lambda}{2*sin\theta_{002}} \quad (5)$$

$$L_c = \frac{k_c\lambda}{FWHM_{002}*cos\theta_{002}} \quad (6)$$

$$L_a = \frac{k_a\lambda}{FWHM_{10}*cos\theta_{10}} \quad (7)$$

$$n_s = \frac{L_c}{d_{002}} \quad (8)$$

$$n_d = 2\left(\frac{L_a}{0.25}\right)^2 \quad (9)$$

where θ_{002} and θ_{10} are the 2 theta angles corresponding to the peak intensities of the 002 and 10 bands respectively, k_c and k_a are Sherrer constants corresponding to 0.91 and 1.84 (Sharma et al. 2000) for 002 and 10 reflection planes respectively, and $FWHM_{002}$ and $FWHM_{10}$ are the full width at half maximum of 002 and 10 reflection planes respectively.

3. Results and Discussion

3.1 Physicochemical Properties and Thermal Stability

Table 1 presents the biopolymer, proximate and ultimate compositions of the commercial cellulose, oil palm frond, oil palm kernel shell and their respective biochars produced at 630 °C in a nitrogen environment. The biopolymer composition for commercial cellulose had no traces of lignin and hemicellulose, whereas oil palm frond and oil palm kernel shell contained mainly of cellulose, hemicellulose and lignin at different proportions respectively. Oil palm frond was highly cellulosic and less lignified compared to oil palm kernel shell. In addition, oil palm frond contained a small amount of extractives, mainly due to the presence of stored simple sugars in its parenchyma tissue (Roslan *et al*., 2014; Zahari *et al*., 2012). As biopolymer thermally decomposed after pyrolysis at 630 °C, the biochars derived from the feedstocks were carbonized with no trace of the biopolymers. The fixed carbon content appeared to correlate with lignin content and increased significantly after carbonization in the increasing order of biochars from commercial cellulose < oil palm frond < oil palm kernel shell. The yield of biochars from commercial cellulose, oil palm frond and oil palm kernel shell was 14.50 %, 32.13 % and 29.70 % respectively. Little variation pertaining to ultimate composition existed among the feedstocks and derived biochars respectively. The carbon content increased significantly from < 47 % in all feedstocks to > 75% after pyrolysis, yielding a highly carbonaceous material. Base on the residual concentration of hydrogen and oxygen and atomic ratio, it was evidence that biochar from commercial

Corresponding author's email address: abubakar.lawal@unimaid.edu.ng

cellulose was highly carbonized and contained the lowest concentration of polar groups compared to biochars from oil palm frond and oil palm kernel.

Table 1: Physicochemical properties of CC, OPF, PKS and their biochars

	CC	OPF	PKS	CC-BC	OPF-BC	PKS-BC
Biochemical composition (%)						
Cellulose	100.00	39.51	20.53	-	-	-
Hemicellulose	0.00	23.56	22.33	-	-	-
Lignin	0.00	23.32	51.54	-	-	-
Extractives	0.00	6.321	0.00	-	-	-
Ultimate composition (%)						
C	39.85	38.58	46.52	78.84	75.57	77.07
H	6.70	6.29	6.07	2.83	2.54	2.66
N	0.02	0.10	0.20	0.19	0.37	0.65
O	52.59	52.35	45.65	8.14	14.38	14.50
H/C	2.00	1.94	1.55	0.43	0.40	0.41
O/C	0.99	1.02	0.74	0.08	0.14	0.14
(O+N)/C	0.99	1.02	0.74	0.08	0.15	0.15
Proximate composition (%)						
FC	6.23	17.86	24.25	77.47	80.89	85.29
VM	92.94	79.47	74.19	12.53	11.96	9.59
Ash	0.84	2.68	1.56	10.00	7.14	5.13

The curves of the thermogravimetric analysis presented in Figure 2 reveal information on the thermal stability of commercial cellulose, oil palm frond and oil palm kernel shell. The mass loss during the main devolatilization stage from 200 to 400 °C (i.e., initial stage) was rapid and followed the order commercial cellulose > oil palm frond > oil palm kernel shell indicating the complete thermal decomposition of polysaccharides. Upon further heating from 400 to 950 °C mass loss continued but at a significantly lower rate. At the temperature range 500 to 950 °C, mass loss of commercial cellulose (3.2 %) was remarkably lowest compared to oil palm frond (6.1 %) and oil palm kernel shell (7.7 %) mainly due to lack of lignin, which would otherwise continue to decompose and release carbon, hydrogen and oxygen in the form of H_2, CO, CO_2, CH_4, C_2H_2 and C_2H_6 at higher temperatures (Yang *et al.* 2006). Thus, analysis of the initial and final pyrolysis stages showed that the thermal stability of the biomass materials followed different order. It is, therefore, reasonable to assume that initial and final mass losses were positively correlated with the content of polysaccharides and lignin respectively. However, the mass losses for their respective biochar were in the opposite order as illustrated in Figure 2 b. This change could be mainly attributed to the catalytic effect of metal oxides formed after production via chemisorption of oxygen (Xu *et al.*, 2019).

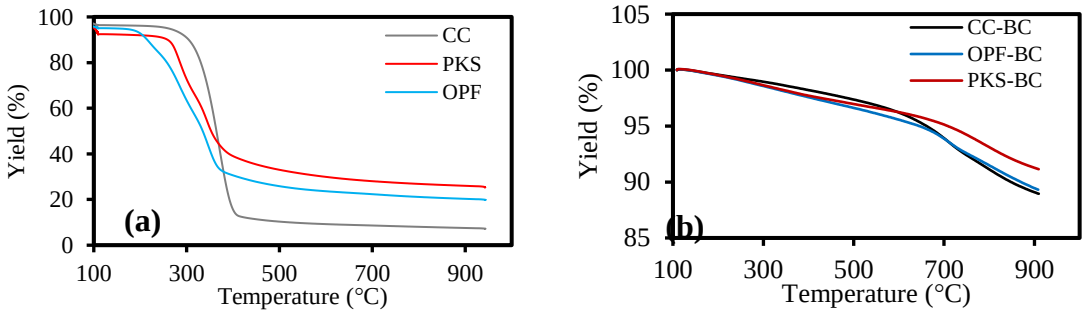

Figure 2: Thermal degradation profile of CC, OPF, PKS and their biochars

The FTIR spectra of the biomass materials and their biochars produced at 630 °C are presented in Figure 3. The wavenumbers of the spectroscopic bands for each spectrum are tabulated in Table 2. The bands corresponding to hydroxyl (O-H), aliphatic (C-H_x), carboxyl (C=O), aromatic skeletal (C=C), carboxylate (C-O-C), phenolic (O-H) and C-O and C-H vibrations and bending of lignocellulosic components were detected with different intensities in commercial cellulose, oil palm frond and oil palm kernel shell. Comparatively, the band attributable to O-H stretch was more intense on the spectrum of commercial cellulose and oil palm frond, which can be related to the higher concentrations of the H-bonded primary alcohols and non H-bonded hydroxyl groups compared to the highly lignified oil palm kernel shell. These functional groups are drastically reduced on the biochars or completely eliminated given ways for new functional groups. New bands at around 3020 1/cm and 888 1/cm attributable to aromatic C-H stretch and out-of-plane deformation (Harvey *et al.*, 2012) were detected due to the presence of aromatic carbon structures in the biochars, and the relative intensities followed the order commercial cellulose > oil palm kernel shell > oil palm frond. Similarly, the

Corresponding author's email address: abubakar.lawal@unimaid.edu.ng

relative intensity of bands at 1636 attributable to aromatic C=O and C=C ring (Abdulrazzaq *et al*., 2014) show that aromaticity in biochar from commercial cellulose was highest while oil palm frond had the least aromatic carbon structure.

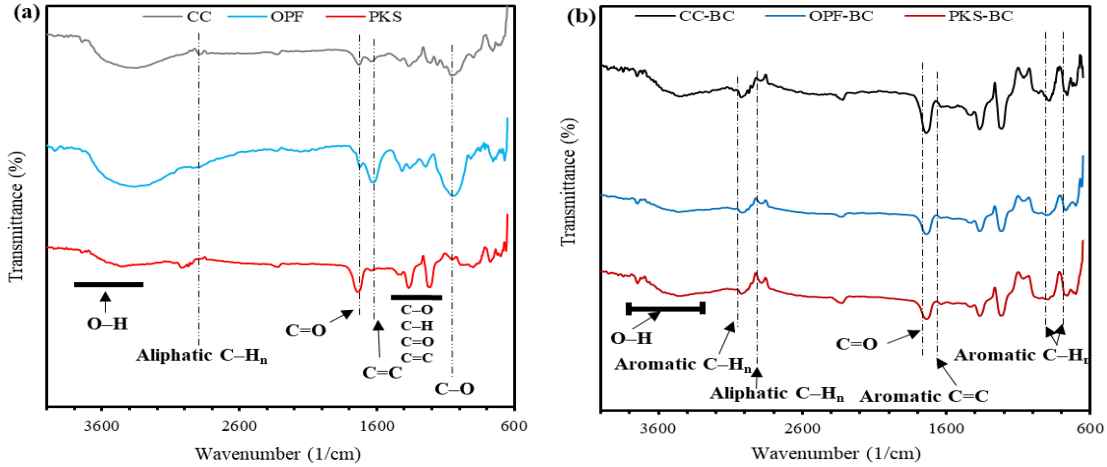

Figure 3: Fourier transform infrared spectra of (a) CC, OPF and PKS and (b) their respective biochars

Table 2: Spectroscopic assignments for raw CC, OPF, PKS and their respective biochar

	Cellulose	Cellulose char	OPF	OPF char	PKS	PKS char
Hydroxyl (-OH) stretch	3353	3466	3363	3456	3370	3463
Aromatic C-H stretch	-	3028	-	3024	3020	3023
Symmetric stretch of aliphatic CH_3	-	2950	-	2950	2973	2950
Asymmetric stretch of aliphatic CH_3	-		-		-	
Symmetric stretch of aliphatic CH_2						
Asymmetric stretch of aliphatic CH_2	2885	2891	-	2883	-	2884
Ester, carboxyl C=O stretching	1731	1740	1724	1739	1740	1738
Aromatic -C=C-, -C=O- stretching	1642	1634	1628	1636	1642	1635
CH, CH_2 and CH_3 deformation	1428	1430	1418	1431	1425	1429
-C-H or O-H bending vibration	1369	1369	1358	1370	1369	1370
C-O-C stretching	1057	1061	1043	1058	1051	1064
Aromatic C-H out-of plane deformation	-	888	-	888	-	895
Aromatic C-H out-of plane deformation	757	760	754	771	776	768

Since part of the formation of aromatic structure in biochar proceeds through the thermal conversion of aliphatic C-H fragments of thermally decomposed lignocellulosic components (Xu *et al*., 2019), further analysis was carried out in the C-H stretch regions to determine the aromaticity calculated from the ratio of aromatic C-H groups to aliphatic C-H groups. The aromaticities of biochar derived from commercial cellulose, oil palm frond and palm kernel shell are presented in Figure 4. The biochar from commercial cellulose had the highest aromaticity reflecting the ease (compared to the other biochars) of converting thermally decomposed aliphatic C-H of cellulosic origin to condensed aromatic structure mainly through dehydration, decarboxylation, dehydrogenation and aromatization processes (Xu *et al*., 2019). Despite the presence of aromatic compounds attributed to lignin in the oil palm kernel shell (Figure 3), the biomass exhibited the lowest aromaticity, possibly due to the high thermal stability of lignin and its decomposed aliphatic C-H components which has to undergo additional demethylation before dehydrogenation and aromatization. In addition, the presence of lignin suppresses the tendency of intramolecular condensation of amorphous char derived from cellulose (Hosoya *et al*., 2007). The inconsistency of the aromaticity with H/C ratio (i.e., degree of carbonization) have been suggested to be due to different arrangement of the elements in the structure of the biochars (Xu *et al*., 2019).

Corresponding author's email address: abubakar.lawal@unimaid.edu.ng

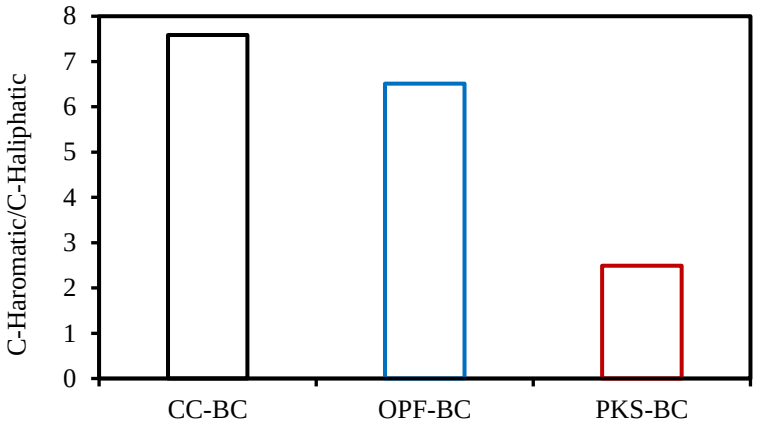

Figure 4: The ratio of the stretch area of aromatic C-H groups to the stretch area of aliphatic C-H groups

The presence of O functional groups give rise to different magnitudes of surface charge on the biochars. Figure 5 presents the PH_{PZC} curves for the biochars obtained from the modified pH drift method. As can be seen, the pH_{PZC} of the biochars were above neutral pH point. The pH_{PZC} of biochar from commercial cellulose was 8.9 while those from oil palm frond and oil palm kernel shell were 9.62 and 9.63 respectively. This was consistent with biochars produced at high temperature having basic surface functional groups (Lopez-Ramon *et al.*, 1999; Xu *et al.*, 2019). In practice, this means that the biochars would have positive charges at pH lower than pH_{PZC} and negative charge at higher values.

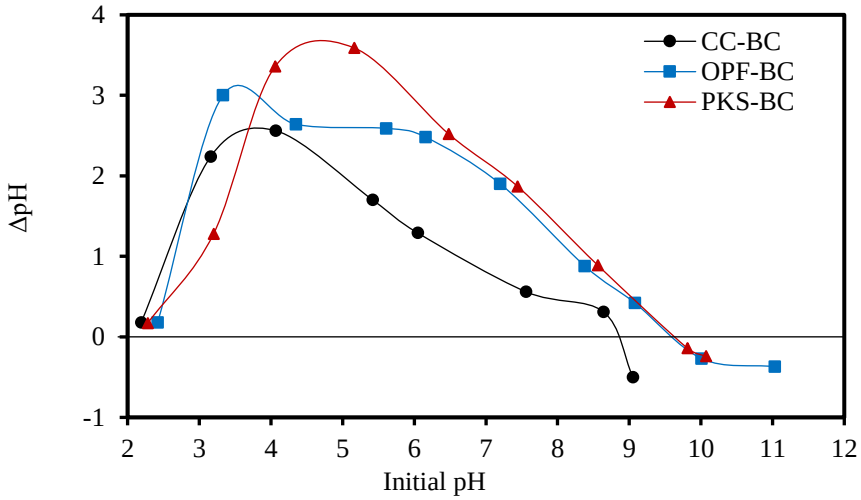

Figure 5: The pH of point of zero charge of biochars from CC, OPF and PKS

3.2 X-ray Diffraction Pattern and Evaluation of Crystallite Parameters

Figure 6 presents the normalized XRD patterns of biochars derived from commercial cellulose, oil palm frond and oil palm kernel shell. The diffraction patterns of the biochars were characterized by a broad diffraction band centred around 2θ = 25°, which correspond to the (002) diffuse graphite band (Wu *et al.*, 2012). The (10) diffraction corresponding to atomic ordering within the graphene sheet (Guerrero *et al.* 2008; Keiluweit *et al.* 2010) was weak and broad for biochars derived from oil palm frond and oil palm kernel shell, while a strong (10) diffraction peak appeared on cellulose. The proportion of disorganized carbons comprises of the aliphatic chains and amorphous carbon. The concentration of the amorphous carbons gave rise to the background intensity of the diffraction profile, while the asymmetry of the (002) band to the left was due to the presence of saturated functional groups attached to the edge of the graphene sheets. The visual assessment of the diffraction profiles in Figure 6 showed that concentration of amorphous carbon in biochar from oil palm kernel shell was the highest, while oil palm frond-derived biochar had the least proportion of amorphous carbon. It is difficult to discern the γ band corresponding to the aliphatic carbon on the (002) band.

Corresponding author's email address: abubakar.lawal@unimaid.edu.ng

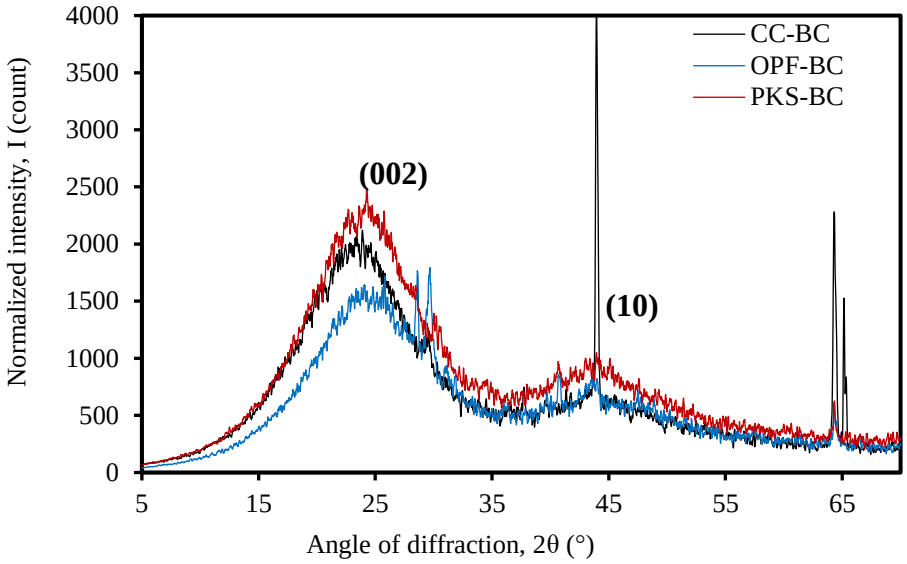

Figure 6: X-ray intensity curves of biochars from CC, OPF and PKS

The diffraction band corresponding to (002) was separately fitted with Pearson IV distribution and the parameters obtained were used to calculate the interlayer spacing, d_{002}, the thickness of the crystallite formed, L_c and the average number of hexagonal layers per stack, n_s, while the average diameter of the crystallites was obtained from (10) diffraction band. Table 3 presents the statistical parameters obtained from curve fitting and the crystallite parameters calculated. The different values of the crystallite structural parameters were an indication of the influence of the nature of the feedstock material and characteristics of the crystallites structure. For instance, the magnitude of d_{002} reveals the degree of crystallites graphitization and as such, the biochars had crystallites with a lower order of graphitization compared to graphite (0.336 nm). The crystallites in biochar from oil palm kernel shell had the highest tendency of graphitizing, whereas crystallites in oil palm frond-derived biochar revealed highly turbostratic characteristics. Presence of low fraction of lignin content in oil palm frond has a deterring effect on graphitization process of crystallites formed, however for high content lignin biomass such as palm kernel shell, lignin encourages graphitization process of the crystallites formed due to the compact conformation of lignin. The diameter of graphene sheets formed in biochar from commercial cellulose was at least 22 times larger than the two biochars from oil palm frond and oil palm kernel shell.

Table 3: Curve fitting and structural crystallite parameters along (002) and (10) X-ray diffraction bands

Crystallite parameters	CC-BC	OPF-BC	PKS-BC
Pearson IV quality of fit R^2	0.9684	0.9643	0.9742
$2\theta_{002}$ (°)	25.44	24.93	25.82
β_{002} (°)	5.16	7.15	5.41
d_{002} (nm)	0.3501	0.3572	0.3451
L_c (nm)	1.60	1.15	1.53
n_s	4.56	3.22	4.42
Gauss quality of fit, R^2	0.9788	0.9548	0.9742
$2\theta_{10}$ (°)	43.97	43.47	43.39
β_{10} (°)	0.27	5.94	6.40
L_a (nm)	64.99	2.95	2.73
n_d	135152	278	239
L_a/L_c	40.62	2.57	1.78

4. Conclusion

The molecular structure of the biochars as suggested by FTIR spectra, atomic ratios and XRD spectra comprised of both amorphous carbons and turbostratic crystallites at different proportion. Generally, the thermal decomposition mechanism for cellulose and lignin differs: cellulose decomposed rapidly to form O heterocyclic rings before final phase transition to graphene sheets at a much lower temperature, whereas lignin decomposed slowly and begins forming graphene sheets after series of condensation reactions at higher temperatures. Cellulose decomposed via dehydration and condensation and forms a low-density relatively volatile chars comprised mainly of levoglucosenone and hydroxymethylfurfural. These oxygenated heterocyclic rings would experience further dehydration, decarboxylation, aromatization and intermolecular condensation to form graphene sheets. On the other hand, lignin decomposed to relatively thermally stable phenolic and

Corresponding author's email address: abubakar.lawal@unimaid.edu.ng

oxygenated aromatic rings and with further dehydration, dehydrogenation and intermolecular condensation, graphene sheets are formed. In practice, biochar derived from highly cellulosic biomass could suitable for adsorption, while lignified derived-biochar could be a suitable catalyst due to it diverse surface functionality.

Acknowledgement

This research was funded by the Fundamental Research Grant Scheme – Malaysia Research Star Award [Grant number: FRGS-MRSA/1/2018/STG07/UPM/01/1]. The authors would like to express their profound appreciation to Universiti Putra Malaysia and Kyushu Institute of Technology for their technical supports.

References

Abd Waft, NS., Lau, HLN., Loh, SK., Abdul Aziz, A., Ab Rahman, Z. and May, CY. 2017. Activated carbon from oil palm biomass as potential adsorbent for palm oil mill effluent treatment. Journal of Oil Palm Research, 29(2): 278–290.

Abdulrazzaq, H., Jol, H., Husni, A., and Abu-Bakr, R. 2014. Characterization and stabilisation of biochars obtained from empty fruit bunch, wood, and rice husk, BioRes. 9(2): 2888-2898.

Ali, AAM., Othman, MR., Shirai, Y. and Hassan, MA. 2015. Sustainable and integrated palm oil biorefinery concept with value-addition of biomass and zero emission system. Journal of Cleaner Production, 91: 96–99.

Amosa, MK., Jami, MS., AlKhatib, MFR., Jimat, DN., and Muyibi, SA. 2014. Comparative and optimization studies of adsorptive strengths of activated carbons produced from steam- and CO_2-activation for BPOME treatment. Advances in Environmental Biology, 8(3): 603–612.

Cantrell, K., Martin, J. and Ro, K. 2010. Application of thermogravimetric analysis for the proximate analysis of livestock wastes. Journal of ASTM International, 7(3): 1–13.

Cao, X., Pignatello, JJ., Li, Y., Lattao, C., Chappell, MA., Chen, N., Miller, LF. and Mao, J. 2012. Characterization of wood chars produced at different temperatures using advanced solid-state 13C NMR spectroscopic techniques. Energy and Fuels, 26(9): 5983–5991.

Guerrero, M., Ruiz, MP., Millera, Á., Alzueta, MU. and Bilbao, R. 2008. Characterization of Biomass Chars Formed under Different Devolatilization Conditions: Differences between Rice Husk and Eucalyptus. Energy and Fuels 22: 1275–1284.

Harvey, OR., Herbert, BE., Kuo, LJ., and Louchouarn, P. 2012. Generalized two-dimensional perturbation correlation infrared spectroscopy reveals mechanisms for the development of surface charge and recalcitrance in plant-derived biochars. Environmental Science and Technology, 46(19): 10641–10650.

Hosoya, T., Kawamoto, H. and Saka, S. 2007. Pyrolysis behaviors of wood and its constituent polymers at gasification temperature. Journal of Analytical and Applied Pyrolysis, 78(2): 328–336.

Jia, Q. and Lua, AC. 2008. Effects of pyrolysis conditions on the physical characteristics of oil-palm-shell activated carbons used in aqueous phase phenol adsorption. Journal of Analytical and Applied Pyrolysis, 83(2): 175–179.

Keiluweit, M., Nico, PS., Johnson, MG. and Kleber, M. 2010. Dynamic molecular structure of plant biomass-derived black carbon (biochar). Environmental Science and Technology, 44(4): 1247–1253.

Kong, SH., Loh, SK., Bachmann, RT., Rahim, SA., and Salimon, J. 2014. Biochar from oil palm biomass: A review of its potential and challenges. Renewable and Sustainable Energy Reviews, 39: 729–739.

Lopez-Ramon, MV., Stoeckli, F., Moreno-Castilla, C., and Carrasco-Marin, F. 1999. On the characterization of acidic and basic surface sites on carbons by various techniques. In Carbon, 37.

Mahmood, T., Saddique, M T., Naeem, A., Westerhoff, P., Mustafa, S. and Alum, A. 2011. Comparison of different methods for the point of zero charge determination of NiO. Industrial and Engineering Chemistry Research, 50(17): 10017–10023.

Norrrahim, MNF., Ariffin, H., Yasim-Anuar, TAT., Ghaemi, F., Hassan, MA., Ibrahim, NA., Ngee, JLH. and Yunus, WMZW. 2018. Superheated steam pretreatment of cellulose affects its electrospinnability for microfibrillated cellulose production. Cellulose, 25: 3853–3859.

Nowicki, P., Kazmierczak, J. and Pietrzak, R. 2015. Comparison of physicochemical and sorption properties of activated carbons prepared by physical and chemical activation of cherry stones. Powder Technology, 269: 312–319.

Parthasarathy, S., Mohammed, RR., Fong, CM., Gomes, RL., and Manickam, S. 2016. A novel hybrid approach of activated carbon and ultrasound cavitation for the intensification of palm oil mill effluent (POME) polishing. Journal of Cleaner Production, 112: 1218–1226.

Roslan, AM., Zahari, MAKM., Hassan, MA., and Shirai, Y. 2014. Investigation of oil palm frond properties for use as biomaterials and biofuels. Tropical Agriculture and Development, 58: 26–29.

Rugayah, AF., Astimar, AA. and Norzita, N. 2014. Preparation and characterisation of activated carbon from palm kernel shell by physical activation with steam. Journal of Oil Palm Research, 26(3): 251–264.

Sharma, A., Kyotani, T. and Tomita, A., 2000. Comparison of structural parameters of PF carbon from XRD and HRTEM techniques. Carbon 38: 1977–1984.

Wu, W., Yang, M., Feng, Q., McGrouther, K., Wang, H,. Lu, H., and Chen, Y. 2012. Chemical characterization of rice straw-derived biochar for soil amendment. Biomass and Bioenergy, 47: 268–276.

Xu, Z., Chen, T., Ding, Z., Hu, X., and Nie., G. 2019. Effects of magnesium impregnation on stability and sorption performance of biochar derived from sawdust and corn husks. BioResources, 14(1): 289-301.

Yang, H., Yan, R., Chen, H., Lee, DH., Liang, DT. and Zheng, C. 2006. Pyrolysis of palm oil wastes for enhanced production of hydrogen rich gases. Fuel Processing Technology, 87(10): 935–942.

Zahari, MAKM., Zakaria, MR., Ariffin, H., Mokhtar, MN., Salihon, J., Shirai, Y. and Hassan, MA. 2012. Renewable sugars from oil palm frond juice as an alternative novel fermentation feedstock for value-added products. Bioresource Technology, 110: 566–571.

Zainal, NH., Aziz, AA., Idris, J., Jalani, NF., Mamat, R., Ibrahim, MF., Hassan, MA. and Abd-Aziz, S. 2018. Reduction of POME final discharge residual using activated bioadsorbent from oil palm kernel shell. Journal of Cleaner Production, 182: 830–837.

Corresponding author's email address: abubakar.lawal@unimaid.edu.ng